Crystal Structures and Thermal and Electrical Properties of the New Silver (poly)Chalcogenide Halides $Ag_{23}Te_{12}Cl$ and $Ag_{23}Te_{12}Br$

Stefan Lange, **Melanie Bawohl**, and **Tom Nilges***

Institut für Anorganische und Analytische Chemie, Universität Münster, Corrensstrasse 30, 48149 Münster, Germany

Two new silver (poly)chalcogenide halides, $Ag_{23}Te_{12}Cl$ and $Ag_{23}Te_{12}Br$, were characterized by powder X-ray phase analysis, energy dispersive X-ray analysis, and crystal structure determinations at various temperatures. Thermal analyses of both compounds and electrochemical measurements for the bromide completed the investigation. The compounds $Ag_{23}Te_{12}X$ (X = Cl, Br) are isostructural and crystallize orthorhombically (space group *Pnnm*, Z = 4) as systematic twins. The lattice parameter values derived from X-ray powder data were $a = 21.214(2)$ Å, $b = 21.218(2)$ Å, $c = 7.7086(7)$ Å, and $V = 3469.8(6)$ Å^3 for $Ag_{23}Te_{12}Cl$ at 293 K and $a = 21.170(1)$ Å, $b = 21.170(1)$ Å, $c = 7.7458(5)$ Å, and $V = 3471.4(4)$ Å^3 for $Ag_{23}Te_{12}Br$ at 298 K. An enhanced silver ion mobility was revealed by impedance spectroscopy investigations. No phase transitions were observed in the temperature range 100−750 K. These two silver(I) (poly)chalcogenide halides are the second set of representatives of a new class of coinage-metal (poly)chalcogenide halides in which both covalently bonded $[Te_2]^{2-}$ dumbbells and ionically bonded Te^{2-} anions appear.

Introduction

Since the discovery of fast ionic conductors such as MAg_4I_5 (M = K, Rb, NH_4)[1] and Na-β-alumina,[2] the research field of solid electrolytes has attracted considerable interest. Ion-conducting materials play a key role in high-technology applications such as lithium batteries, fuel cells, and gas sensors. Very recently, silver ion conductors were drawn into the focus of materials scientists as possible electrolytes for nonvolatile data storage modules. Nanoscale silver spots that are reversibly generated and dissolved within thin films of a solid silver electrolyte are used in order to switch between on and off states in so-called programmable metallization cells, one possible next-generation memory device technology.[3] Optimization of known systems and the continuous search for new compounds are necessary in order to meet the ever-increasing demands of modern applications.

In our previous work on solid silver electrolytes, we showed that chemical substitution in the anionic substructure of silver chalcogenide halides is an appropriate means for influencing their physical properties, such as phase transition temperatures and electrical conductivity.[4] During investigations of the ternary systems Ag–Q–X (Q = S, Se, Te; X = Cl, Br, I), we were able to prepare the new solid electrolyte $Ag_{10}Te_4Br_3$.[5,6] This was the first ternary compound from the AgQX system that contained both ionic and covalent building blocks in its chalcogen substructure, placing it within the phase field $AgX–Ag_2Q–Q$. Because this compound contains both polymeric motifs and isolated tellurium atoms, we have called this new class of compounds silver (poly)chalcogenide halides.

Tetramorphic $Ag_{10}Te_4Br_3$ features isolated Te^{2-} ions and Te_2^{2-} dumbbells in its (poly)telluride substructure. So-called Te_4 units are formed by a dumbbell and two additional neighboring tellurium atoms. Pronounced silver mobility was found in the proximity of these Te_4 units in all of the

---

* Corresponding author. Phone: +49-251-83-36645. Fax: +49-251-83-36636. E-mail: nilges@uni-muenster.de.

(1) (a) Bradley, J. N.; Greene, P. D. *Trans. Faraday Soc.* **1966**, *62*, 2069–2075. (b) Bradley, J. N.; Greene, P. D. *Trans. Faraday Soc.* **1967**, *63*, 424–430.
(2) Yao, Y.-F. Y.; Kummer, J. T. *J. Inorg. Nucl. Chem.* **1967**, *29*, 2453–2475.
(3) Kozicki, M. N.; Mitkova, M.; Park, M.; Balakrishnan, M.; Gopalan, C. *Superlattices Microstruct.* **2003**, *34*, 459–465.
(4) (a) Nilges, T.; Dreher, C.; Hezinger, A. *Solid State Sci.* **2005**, *7*, 7988. (b) Nilges, T.; Lange, S. *Z. Anorg. Allg. Chem.* **2005**, *631*, 3002–3012. (c) Nilges, T.; Bawohl, M.; Lange, S. *Z. Naturforsch.* **2007**, *62b*, 955–964.
(5) Lange, S.; Nilges, T. *Chem. Mater.* **2006**, *18*, 2538–2544.
(6) Lange, S.; Bawohl, M.; Wilmer, D.; Meyer, H.-W.; Wiemhöfer, H.-D.; Nilges, T. *Chem. Mater.* **2007**, *19*, 1401–1410.

polymorphs.[6] This finding indicated that the coexistence of covalent and ionic building blocks accounts for favorable physical properties. Thus, the question arose whether other silver (poly)chalcogenide halides exist.

The ternary systems AgTeCl and AgTeBr have previously been studied by several research groups.[7] Blachnik and Dreisbach[8] reported on a possible high-temperature phase (containing about 20% AgBr) in the AgTeBr system but did not specify any details on its exact composition or structure. Schnieders[9] described a phase with the estimated composition $Ag_{21}Te_{10}Br$ and reported that it crystallizes tetragonally in either the *P4/mnc* or *P4nc* space group, but a complete structure description was not given.

The uncertainties and partially contradicting statements in the literature were reason for us to start a reinvestigation of these systems. After systematic research, we were able to find and characterize two new representatives of the aforementioned silver (poly)chalcogenide halide structure family. In this paper, we report on the synthesis, crystal structures, and thermal and electrical properties of $Ag_{23}Te_{12}Cl$ and $Ag_{23}Te_{12}Br$.

Experimental Section

Synthesis. $Ag_{23}Te_{12}Cl$ and $Ag_{23}Te_{12}Br$ were prepared from mixtures of silver (Chempur, 99.9%) and tellurium (Chempur, 99.999%) with silver(I) chloride (Alfa Aesar, 99.9%) and silver(I) bromide (Chempur, 99+%), respectively, in the molar ratio 22:12:1. The total mass was approximately 1 g in each case. The reaction mixtures were sealed in evacuated silica ampoules, heated to 1220 K for 1 day, and quenched in an ice bath. The crude products were then finely ground, again sealed in evacuated silica ampoules, and annealed at 640 K ($Ag_{23}Te_{12}Cl$) or 650 K ($Ag_{23}Te_{12}Br$) for two weeks. Rod-shaped, black single crystals were isolated from the reaction products.

$RbAg_4I_5$, used for electron-blocking electrodes in the impedance spectroscopy measurements, was prepared by mixing AgI (Sigma-Aldrich, 99%) and RbI (Alfa Aesar, 99.8%) in a 4:1 molar ratio in evacuated silica ampoules, followed by heating to 970 K and quenching in an ice bath. $RbAg_4I_5$ was stored at 320 K prior to use, and each electrode was prepared immediately before the measurement. The phase purity of $RbAg_4I_5$ was checked by powder X-ray diffraction experiments and energy dispersive X-ray (EDX) analyses before use.

Thermal Analysis. Differential scanning calorimetry (DSC) measurements were performed using a Netzsch DSC 204t calorimeter under a nitrogen atmosphere in aluminum crucibles for temperatures up to 500 K and silica ampoules for temperatures above 500 K. Hg, In, Sn, Bi, Zn, and CsCl were used for calibration. A temperature accuracy of ±1 K for onset values was estimated from the calibration measurements. A temperature range of 140–750 K was applied, and the heating rate was 10 K/min. At least two consecutive runs were conducted in order to check the reversibility of the observed effects. A standard deviation of 2 K was estimated for the derived values.

Impedance Spectroscopy. Partial ionic conductivities were measured using a symmetrical setup involving two electron-blocking, silver ion-conducting $RbAg_4I_5$ electrodes, according to well-known electrochemical concepts introduced by Wagner[10] and applied by many others since then.[6,11] Details about the electrode/sample setup are given elsewhere.[6] A cold pressed pellet of $Ag_{23}Te_{12}Br$ was mounted on $RbAg_4I_5$ electrode pellets and contacted to platinum electrodes via pressed silver powder in order to achieve a symmetrical setup. The whole unit was mounted to a homemade measuring cell and transferred into a Julabo MW4 temperature control unit. A Solartron 1260 frequency response analyzer and a Solartron 1287 potentiostat were used to record impedance spectra under a nitrogen atmosphere in the temperature range 309–395 K over a frequency range of 1 MHz–0.1 Hz. An equilibration time of 1 h of between each set of measurements was allowed in order to achieve a constant temperature at the sample. After each set of impedance measurements at a particular temperature, a direct-current (dc) measurement was performed by applying a dc potential difference (±10 mV) and recording the steady-state ionic current after 400 s. The resulting resistance was used to calculate the ionic conductivity. The agreement of the ionic conductivities derived from the low-frequency part of the impedance spectra with those obtained from the dc steady-state current was well within the estimated errors of the experiments.

Powder X-ray Diffraction. Powder X-ray phase analysis was performed using a Stoe Stadi-P X-ray powder diffractometer operated with Ge-monochromated Cu $K\alpha_1$ radiation ($\lambda = 1.54051$ Å) and equipped with a linear 5° position-sensitive detector in transmission geometry. Silicon was used as an external standard. The measurements were carried out at 293(1) and 298(1) K for $Ag_{23}Te_{12}Cl$ and $Ag_{23}Te_{12}Br$, respectively. All of the powder X-ray data were indexed, and unit cell parameters were refined using the Stoe WinXpow program package.[12]

Single-Crystal X-ray Diffraction. Intensity data from selected single crystals were collected on a Stoe IPDS II diffractometer fitted with Mo $K\alpha$ radiation ($\lambda = 0.71073$ Å) at various temperatures. During data collection, the temperature was controlled using a Cryostream Plus system (Oxford). Temperature calibration was achieved using the two reversible phase transitions of Ag_5Te_2Cl at 244 and 334 K;[13] measured temperatures showed a deviation of less than ±0.2 K from the ideal values. All of the data sets were corrected for Lorentz, polarization, and absorption effects. The programs X-RED and X-SHAPE[14] were used to optimize the crystal shape from symmetry-equivalent reflections in order to perform a numerical absorption correction. Space groups were derived from the systematic extinctions. Reconstructed precession photographs in reciprocal space were carefully examined for possible super-structure reflections. The crystal structures were solved by direct methods[15] and refined using a nonharmonic Gram–Charlier ap-

(7) (a) Blachnik, R.; Kudermann, G. *Z. Naturforsch.* **1973**, *28b*, 1–4. (b) Bontschewa-Mladenowa, Z.; Aramov, N.; Rajkowa, D. *Z. Anorg. Allg. Chem.* **1973**, *402*, 306–312. (c) Karbanov, S.; Bontschewa-Mladenowa, Z.; Aramov, N. *Monatsh. Chem.* **1972**, *103*, 1496–1502.
(8) Blachnik, R.; Dreisbach, H. A. *J. Solid State Chem.* **1985**, *60*, 115–122.
(9) Schnieders, F. Ph.D. Thesis, University of Düsseldorf, 1995.
(10) Wagner, C. *J. Chem. Phys.* **1953**, *21*, 1819.
(11) (a) Janek, J.; Korte, C. *Solid State Ionics* **1996**, *92*, 193–204. (b) Rickert, H.; Wagner, C. *Ber. Bunsenges. Phys. Chem.* **1963**, *67*, 621–629.
(12) *WinXPow*, version 1.08; Stoe & Cie GmbH: Darmstadt, Germany, 2000.
(13) Nilges, T.; Nilges, S.; Pfitzner, A. *Chem. Mater.* **2004**, *16*, 806–812.
(14) *X-RED and X-SHAPE, Programs for Absorption Correction*, versions 1.31 and 2.07; Stoe & Cie GmbH: Darmstadt, Germany, 2005.
(15) Sheldrick, G. M. *SHELXS97*; University of Göttingen: Göttingen, Germany, 1997.
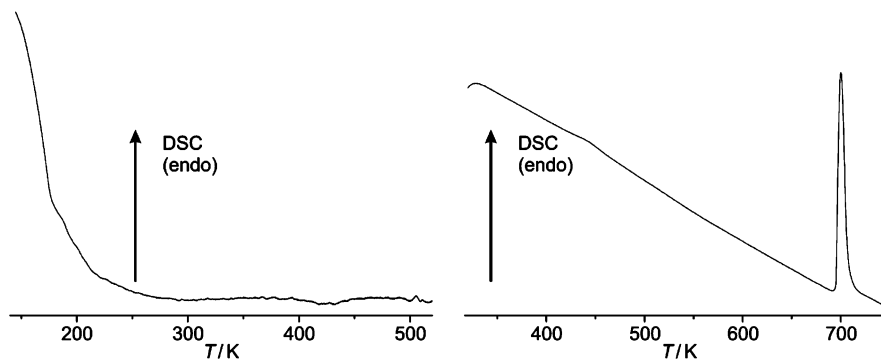
Figure 1. DSC measurements on $Ag_{23}Te_{12}Br$. In the low-temperature region (left), no effects were observed. The high-temperature region (right) shows one endothermic effect, which was assigned to the peritectic decomposition point.

proach[16] for the description of the highly disordered silver substructure. A 3σ cutoff was applied to the third-order displacement parameters.

EDX Measurements. Semiquantitative EDX analyses were carried out using a Leica 420i scanning electron microscope fitted with an energy dispersive detector (Oxford). Ag, HgTe, KBr, and KCl were used as standards for calibration. A voltage of 20 kV was applied to the samples.

Results and Discussion

The structures of the new compounds $Ag_{23}Te_{12}Cl$ and $Ag_{23}Te_{12}Br$ were determined by X-ray diffraction using powders and single crystals. Additionally, $Ag_{23}Te_{12}Br$ was characterized by thermal analysis and impedance spectroscopy. Both compounds were stable with respect to light and moisture for more than a month and could be handled in air under standard conditions.

Thermal Analysis. The thermal properties of $Ag_{23}Te_{12}X$ were examined over the temperature range $140-750$ K by differential scanning calorimetry. Measured thermograms for $Ag_{23}Te_{12}Br$, which are illustrated in Figure 1, showed one endothermic effect at an onset temperature of 690 K. No further effects that could point to structural phase changes were observed in the investigated temperature range. Subsequent powder X-ray phase analysis identified the thermal effect as the peritectic reaction to form $Ag_{2}Te$[17] and an additional unidentified phase. Qualitatively similar results were obtained for $Ag_{23}Te_{12}Cl$, which decomposed peritectically at 734 K to yield $Ag_{2}Te$[17] and $Ag_{5}Te_{2}Cl$.[8,13]

Phase Analyses: EDX and Powder X-ray Diffraction. Semiquantitative EDX analyses were used in order to determine the approximate compositions of the compounds. The measured values are summarized in Table 1. The results for $Ag_{23}Te_{12}X$ (X = Cl, Br) agree well with the calculated values within the expected errors of the method.

Powder X-ray diffractograms of $Ag_{23}Te_{12}Cl$ and $Ag_{23}Te_{12}$-Br were measured at room temperature. Comparisons of measured and calculated powder patterns for both compounds are given in Figure 2. The diffractogram of $Ag_{23}Te_{12}Cl$ contained two reflections having *d* spacings similar to those

(16) (a) Petricek, V.; Dusek, M.; Palatinus, L. *JANA2000, The Crystallographic Computing System*; Institute of Physics: Praha, Czech Republic, 2000. (b) Zucker, U. H.; Schulz, H. *Acta Crystallogr.* **1982**, *A38*, 563–568. (c) Kuhs, W. F. *Acta Crystallogr.* **1992**, *A48*, 80–98.
(17) Schneider, J.; Schulz, H. *Z. Kristallogr.* **1993**, *203*, 1–15.

Table 1. EDX Analyses of $Ag_{23}Te_{12}X$ (X = Cl, Br)[a]

compound	Ag	Te	X
$Ag_{23}Te_{12}X$ (calculated)	63.9	33.3	2.8
$Ag_{23}Te_{12}Cl$	62(2)	33(2)	5(2)
$Ag_{23}Te_{12}Br$	63(2)	32(2)	5(2)

[a] Values (atom %) were averaged over 3−10 measurements. Estimated standard deviations are given in parentheses.
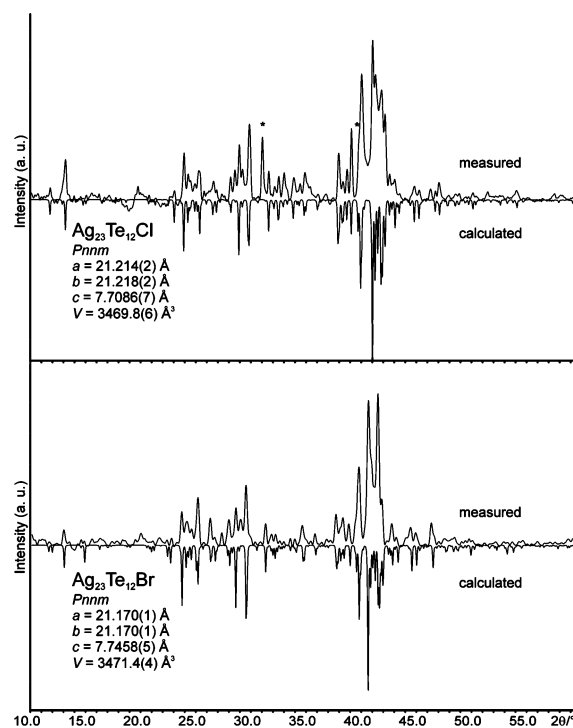
Figure 2. Measured (at 298 K) and calculated powder X-ray diffractograms of (top) $Ag_{23}Te_{12}Cl$ and (bottom) $Ag_{23}Te_{12}Br$. The reflections marked with asterisks in the top panel are due to impurities of $Ag_{2}Te$. The calculated patterns derived from the single-crystal structure determinations are drawn with negative intensities for ease of comparison.

of the two strongest reflections of monoclinic $Ag_{2}Te$.[17] No impurities were found for $Ag_{23}Te_{12}Br$. The reflections of both compounds could be indexed and refined with an orthorhombic unit cell. The resulting lattice parameters are listed in Table 2. The values obtained for *a* and *b* are equal within the standard deviations, indicating a pseudotetragonal unit cell. The lattice parameters of $Ag_{23}Te_{12}Br$ were very close to the values reported by Schnieders[9] for the postulated compound $Ag_{21}Te_{10}Br$. Given the very similar composition, it is likely that Schnieders was actually characterizing the

Table 2. Lattice Parameters for $Ag_{23}Te_{12}X$ (X = Cl, Br) Determined by Powder or Single-Crystal X-ray Diffraction at Various Temperatures[a]

compound	a (Å)	b (Å)	c (Å)	V (Å³)	T (K)	reference
$Ag_{23}Te_{12}Cl$	21.214(2)	21.218(2)	7.7086(7)	3469.8(6)	298	this work
$Ag_{23}Te_{12}Br$	21.170(1)	21.170(1)	7.7458(5)	3471.4(4)	298	this work
$Ag_{23}Te_{12}Br$	21.152(2)	21.152(2)	7.7591(6)	3471.1(5)	293	this work[b]
$Ag_{23}Te_{12}Br$	21.074(1)	21.074(1)	7.732(1)	3433.8(3)	150	this work[b]
$Ag_{23}Te_{12}Br$	21.055(1)	21.055(1)	7.724(1)	3424.2(3)	100	this work[b]
$Ag_{21}Te_{10}Br$	21.166(3)		7.806(1)	3497(1)	298	9[b]
$Ag_{21}Te_{10}Br$	21.067(11)		7.778(4)	3452(1)	143	9[b]

[a] Standard deviations are given in parentheses. Values for the postulated compound $Ag_{21}Te_{10}Br$[9] are given for comparison. [b] Lattice parameters were obtained from single-crystal data.

Table 3. Crystallographic Data and Refinement Details for $Ag_{23}Te_{12}X$ (X = Cl, Br) (Data for a Refinement in Space Group $P4/mnc$, a Supergroup of $Pnnm$, Are Given for $Ag_{23}Te_{12}Br$ in Order To Show the Differences between the Two Refinements)

compound	$Ag_{23}Te_{12}Cl$	$Ag_{23}Te_{12}Br$	$Ag_{23}Te_{12}Br$
structure type	$Ag_{23}Te_{12}Br$ type	$Ag_{23}Te_{12}Br$ type	$Ag_{23}Te_{12}Br$ type
molar mass (g mol⁻¹)	4047.7	4092.1	4092.1
crystal size (mm³)	0.04 × 0.03 × 0.02	0.08 × 0.06 × 0.04	0.08 × 0.06 × 0.04
crystal color	dark gray	dark gray	dark gray
crystal system	orthorhombic	orthorhombic	orthorhombic
space group	$Pnnm$	$Pnnm$	$P4/mnc$
lattice parameters			
a (Å)	21.214(2)	21.152(2)	21.152(2)
b (Å)	21.218(2)	21.152(2)	21.152(2)
c (Å)	7.7086(7)	7.7591(6)	7.7591(6)
V (Å³)	3472.7(5)	3471.4(5)	3471.4(5)
Z	4	4	4
ρ_{calc} (g cm⁻³)	7.75	7.83	7.83
diffractometer		Stoe IPDS II	
radiation		Mo Kα (0.71073 Å), graphite monochromator	
absorption correction		numerical[a]	
T (K)	298	293	−
no. of independent reflections	3397	3884	1990
R_{int} (all)	0.1376	0.0509	0.0568
refinement		least-squares on F^2 [b]	−
R [$I > 3\sigma(I)$]	0.0204	0.0404	0.0825
R_w [$I > 3\sigma(I)$]	0.0181	0.0461	0.1124
R (all)	0.1049	0.1167	0.1443
R_w (all)	0.0307	0.0565	0.1169
no. of parameters	544	433	205
goodness of fit (all)	0.70	1.08	3.90
twin matrix		(0 −1 0; 1 0 0; 0 0 1)	−
BASF	0.496(1)	0.497(2)	−
residual electron density max, min (e Å⁻³)	0.88, −0.65	0.83, −1.03	3.20, −2.69

[a] Using the programs X-RED and X-SHAPE.[14] [b] Using JANA2000.[16]

same compound as in our experiment. All attempts to prepare $Ag_{21}Te_{10}Br$ in our lab failed.

Single-Crystal X-ray Structure Determination. Intensity data for selected single crystals of $Ag_{23}Te_{12}Cl$ and $Ag_{23}Te_{12}Br$ were collected in order to determine their crystal structures. All of the reflections could be indexed with orthorhombic unit cells in both cases, and the resulting lattice parameters agreed with the values obtained by powder diffraction within the expected errors. A pseudotetragonal symmetry can be derived directly from the lattice parameters, and the automatic cell search routine of the diffractometer proposed a tetragonal unit cell in both cases. For $Ag_{23}Te_{12}Br$, the small difference between the unit cell parameters at 298 K (powder X-ray diffraction experiment) and 293 K (single-crystal X-ray diffraction measurement) reflects the sensitivity of these parameters to temperature and the large change in silver mobility over a small temperature range. Accordingly, the temperature during the single-crystal structure determinations was kept constant with an accuracy of ±0.2 K using a temperature controller (Oxford Cryostream Plus). We decided to use the lattice parameters derived directly from the single-crystal data for $Ag_{23}Te_{12}Br$ in order to make them comparable

to the low-temperature data. No powder X-ray data were determined below room temperature. The lattice parameters for $Ag_{23}Te_{12}Cl$ were derived from powder X-ray data. The space groups of $Ag_{23}Te_{12}Cl$ and $Ag_{23}Te_{12}Br$ were determined after careful analysis of the systematic extinctions based on the pseudotetragonal cell, which led to space group $P4/mnc$, followed by a structure solution using direct methods[15] and subsequent symmetry reduction to $Pnnm$. Enlargement of the unit cell starting from space group $P4/mnc$ [klassengleiche transition of index 3 (k3) to $P4/mnc$] or $Pnnm$ (k3 to $Pnnm$) was not possible because no superstructure reflections were found. We then checked all possible maximal translationengleiche reductions from the supergroup $P4/mnc$ (No. 128) to space groups No. 118, 114, 104, 90, 83, 66, and 58, and the reduction to $Pnnm$ (No. 58) led to a significantly better description of the structure. A comparison of the atomic coordinates of the anion substructures featuring the differences of the two models is given in Table 9 in the Supporting Information. In addition, a further symmetry reduction leading to decoupling (splitting of the 8h into two independent fourfold sites) of the Te6a and Te6b positions was performed. We tested all possible translationengleiche

Table 4. Crystallographic Data and Refinement Details for $Ag_{23}Te_{12}Br$ at 150.0(2) and 100.0(2) K

compound	$Ag_{23}Te_{12}Br$	
molar mass (g mol⁻¹)	4092.1	
crystal size (mm³)	0.08 × 0.06 × 0.04	
crystal color	dark gray	
crystal system	orthorhombic	
space group	*Pnnm*	
lattice parameters		
a (Å)	21.0740(9)	21.055(1)
b (Å)	21.0740(9)	21.055(1)
c (Å)	7.7319(4)	7.7241(4)
V (Å³)	3433.8(3)	3424.2(3)
Z	4	4
ρ_{calc} (g cm⁻³)	7.91	7.94
diffractometer	Stoe IPDS II	
radiation	Mo Kα (0.71073 Å), graphite monochromator	
absorption correction	numerical[a]	
T (K)	150	100
no. of independent reflections	3863	3855
R_{int} (all)	0.0427	0.0463
refinement	least-squares on F^2 [b]	
R [$I > 3\sigma(I)$]	0.0580	0.0451
R_w [$I > 3\sigma(I)$]	0.0699	0.0501
R (all)	0.0893	0.0957
R_w (all)	0.0748	0.0577
no. of parameters	542	559
goodness of fit (all)	3.12	1.66
twin matrix	(0 −1 0; 1 0 0; 0 0 1)	
BASF	0.500(2)	0.500(2)
residual electron density max, min (e Å⁻³)	2.10, −2.10	1.49, −1.54

[a] Using the programs X-RED and X-SHAPE.[14] [b] Using JANA2000.[16]

reductions from *Pnnm* to lower-symmetry space groups (No. 34, 31, 18, 14, and 10), none of which improved the structure description.

A description of the structure using space group *P4/mnc*, a supergroup of *Pnnm*, could also be ruled out on the basis of chemical-structure and statistical considerations (see below). After the aforementioned symmetry reduction followed by several refinement cycles, a structure model with 12 tellurium sites, 1 halogen site, and a large number of partially occupied silver sites could be obtained. A free refinement of all of the silver occupancy factors confirmed the postulated silver content and the composition of Ag_{23}-$Te_{12}X$ within two times the standard deviation. Therefore, the sum of the silver occupancy factors was restricted to the ideal value in the final refinement cycles. The same trend was found for the covalently bonded telluride substructure (Te6a and Te6b, half-occupied positions), and the sum of the occupancy factors was also restricted to 1. In view of the covalently bonded anion substructure, the $Ag_{23}Te_{12}X$ compounds can be written as $(Ag^+)_{23}(Te^{2-})_{10}(Te_2^{2-})(X^-)$. Selected crystallographic data are summarized in Tables 3–6.

The relatively large final R values indicated a crystallographically incorrect description of the structure in space group *P4/mnc*. Additional crystallographic data for the refinement are given in Table 3 for comparison. The fact that for both compounds the a and b lattice parameters were almost equal pointed toward the possibility of twinning. After introduction of the twin matrix (0 −1 0; 1 0 0; 0 0 1), the reliability factors decreased significantly. The twin law corresponds to a *translationengleiche* symmetry reduction

of index 2 (t2) from *P4/mnc* to the subgroup *Pnnm*. This transition leads to a splitting of the 16-fold Te6 site into two 8-fold sites, as illustrated schematically in Figure 3.

A tentative refinement in the higher-symmetry supergroup *P4/mnc* as well as in *Pnnm* led to almost equivalent structure models. Nevertheless, significantly better values of statistical parameters, such as R, goodness of fit, and residual electron density, and a better description of the polyanion substructure (see below) clearly favor the description given by space group *Pnnm*. In order to check for a possible ordering of the silver atoms at low temperatures, we carried out additional single-crystal structure determinations of $Ag_{23}Te_{12}Br$ at 150 and 100 K. In both cases, the structure model derived from the room-temperature measurement was confirmed. We found no evidence for an ordering of silver within the silver substructure. This finding is consistent with the thermal analysis results, which also showed no signs of phase transitions in the temperature range under discussion.

The anion substructures of both $Ag_{23}Te_{12}Cl$ and $Ag_{23}Te_{12}$-Br contain half-occupied tellurium sites (Te6a and Te6b). The interatomic distance between those positions is less than 1 Å and therefore not meaningful. Also, some short AgTe distances related to those positions can be observed. Careful analysis of the reciprocal space gave no evidence for a possible overlooked superstructure that might lead to this kind of artifact. Further symmetry reduction together with the introduction of additional twin laws did not result in removal of the split position. A brief discussion of this aspect was given earlier in this section.

Detailed information on anisotropic displacement parameters and selected interatomic distances can be found in the Supporting Information. Additional information can be obtained from the FIZ Karlsruhe (www.fiz-karlsruhe.de) on quoting the depository numbers CSD 418636 ($Ag_{23}Te_{12}Cl$, 298 K), CSD 418637 ($Ag_{23}Te_{12}Br$, 293 K), CSD 418638 ($Ag_{23}Te_{12}Br$, 150 K), and CSD 418639 ($Ag_{23}Te_{12}Br$, 100 K).

Structure Description. In accordance with our previous reports on (poly)chalcogenide halides, we choose to describe the crystal structures of $Ag_{23}Te_{12}Cl$ and $Ag_{23}Te_{12}Br$ by separating the anion and cation substructures. A topological approach that takes into account interatomic distances that are close to or even slightly greater than the sum of the tellurium van der Waals radii is used to illustrate the anion substructures. The crystal structure of $Ag_{23}Te_{12}X$ (X = Cl, Br) is shown in Figure 4 using this topological approach. The telluride substructure (Te1a to Te5b) can be described by honeycomb-like distorted 6³-nets, a structure motif known from $Ag_{10}Te_4Br_3$.[5,6] Unlike the ones in $Ag_{10}Te_4Br_3$, these nets are puckered in $Ag_{23}Te_{12}X$ (X = Cl, Br) and interpenetrate each other, forming a dihedral angle close to 90° at each interpenetration or contact point. In neither compound are any contacts less than the sum of the van der Waals radii

(18) Maier, J. *Mater. Res. Bull.* **1985**, *20*, 383–392.
(19) Kawamura, J.; Shimoji, M. *Solid State Ionics* **1981**, *3/4*, 41–44.
(20) Reuter, B.; Hardel, K. *Ber. Bunsenges. Phys. Chem.* **1966**, *70*, 82–86.
(21) Takahashi, T.; Ikeda, S.; Yamamoto, O. *J. Electrochem. Soc.* **1972**, *119*, 477–482.
(22) Bärnighausen, H. *MATCH* **1980**, *9*, 139–175.

Table 5. Site Occupancy Factors (sof), Atomic Parameters, and Isotropic Displacement Parameters (U_{iso}) for $Ag_{23}Te_{12}Cl$ at 298 K

atom	Wyckoff site	sof	x	y	z	U_{iso} (Å²)
Te1a	4g	1	0.11880(19)	0.1268(2)	0	0.0366(13)
Te1b	4g	1	−0.1294(2)	0.11853(20)	0	0.0396(13)
Te2a	4g	1	0.1658(2)	0.0374(2)	$^1/_2$	0.0440(15)
Te2b	4g	1	−0.0363(2)	0.1661(2)	$^1/_2$	0.0423(14)
Te3a	4g	1	0.1557(2)	0.2727(2)	$^1/_2$	0.0541(15)
Te3b	4g	1	−0.2706(3)	0.1571(2)	$^1/_2$	0.0586(17)
Te4a	4g	1	0.3958(2)	−0.0019(2)	$^1/_2$	0.0555(17)
Te4b	4g	1	0.0006(2)	0.39442(19)	$^1/_2$	0.0496(16)
Te5a	4g	1	0.0152(3)	0.3009(2)	0	0.0560(16)
Te5b	4g	1	−0.2984(2)	0.0148(2)	0	0.0558(16)
Te6a	8h	0.510(17)	0.3206(3)	0.1797(3)	−0.3177(11)	0.052(3)
Te6b	8h	0.490(17)	−0.1836(3)	0.3191(3)	−0.3124(11)	0.044(3)
Cl	4e	1	0	0	0.2472(9)	0.061(4)
Ag1	8h	0.471(18)	0.0130(12)	0.4272(6)	0.1568(19)	0.161(7)
Ag2	8h	0.491(17)	−0.4224(5)	−0.0103(9)	0.1325(18)	0.133(5)
Ag3	4g	0.241(19)	0.0792(17)	−0.0495(13)	$^1/_2$	0.087(10)
Ag4	4g	0.37(3)	0.0476(13)	0.0751(18)	$^1/_2$	0.188(17)
Ag5	8h	0.379(15)	0.0406(8)	0.2719(4)	−0.3362(16)	0.108(5)
Ag6	8h	0.70(2)	−0.2628(10)	0.0505(7)	−0.323(2)	0.286(9)
Ag7	8h	0.225(12)	−0.0802(7)	0.2305(8)	0.1999(18)	0.050(5)
Ag8	8h	0.32(2)	−0.2797(18)	−0.0578(9)	0.301(3)	0.091(9)
Ag9	8h	0.67(2)	−0.3838(6)	0.1157(10)	−0.202(7)	0.49(2)
Ag10	8h	0.358(16)	0.1827(8)	0.1606(9)	−0.2933(15)	0.072(5)
Ag11	8h	0.62(2)	−0.1775(12)	0.1932(5)	−0.279(3)	0.332(11)
Ag12	8h	0.548(17)	0.0727(7)	0.2003(10)	−0.268(2)	0.214(7)
Ag13	8h	0.165(18)	0.2944(17)	0.076(2)	−0.454(9)	0.047(12)
Ag14	8h	0.53(2)	−0.0624(8)	0.2782(9)	−0.355(4)	0.299(13)
Ag15	8h	0.366(16)	0.4300(5)	0.1112(7)	−0.343(2)	0.129(6)
Ag16	8h	0.286(14)	−0.1212(14)	0.4313(16)	−0.297(4)	0.152(12)
Ag17	8h	0.465(17)	0.0658(7)	0.1205(10)	−0.317(2)	0.181(8)
Ag18	8h	0.329(13)	−0.1412(9)	0.1010(9)	−0.3627(19)	0.184(8)
Ag19	8h	0.44(2)	0.1845(9)	0.2242(8)	−0.149(2)	0.189(7)
Ag20	8h	0.318(17)	−0.1956(9)	0.2241(10)	−0.086(3)	0.252(12)
Ag21	4g	0.30(5)	0.1126(19)	0.0031(14)	0	0.24(6)
Ag22	4g	0.43(3)	−0.0023(10)	0.1038(7)	0	0.252(11)
Ag23	8h	0.55(2)	0.2238(11)	0.0732(11)	−0.844(3)	0.242(11)
Ag24	8h	0.413(17)	−0.0255(9)	0.1800(8)	−0.893(3)	0.218(10)
Ag25	8h	0.49(3)	0.142(2)	−0.0093(8)	−0.1822(16)	0.233(11)
Ag26	4g	0.41(4)	0.4018(14)	0.168(4)	$^1/_2$	0.42(5)
Ag27	4g	0.37(3)	−0.1207(10)	0.4049(14)	$^1/_2$	0.236(12)
Ag28	4g	0.26(2)	0.253(5)	0.220(2)	0	0.30(4)
Ag29	4g	0.305(12)	0	$^1/_2$	0.269(3)	0.129(12)
Ag30	8h	0.501(19)	0.2155(17)	0.3693(6)	−0.3483(18)	0.293(13)
Ag31	8h	0.34(2)	−0.3717(17)	0.2384(8)	−0.329(4)	0.258(13)
Ag32	4g	0.3(2)	0.200(2)	0.1536(10)	$^1/_2$	0.37(3)

of the anions that might point toward any kind of interaction due to this interpenetration.

Te6a and Te6b, representing the polyanion substructure, are located within the anion substructure in such a way that two closely neighbored, half-occupied positions are arranged almost linearly along the c axis (see Figure 3). This arrangement is identical to parts of the anion substructure in $Ag_{10}Te_4Br_3$, the first representative of a (poly)chalcogenide halide.[6] It seems to be obvious that the polychalcogenide substructures in $Ag_{10}Te_4Br_3$ and $Ag_{23}Te_{12}X$ are characterized by comparable structural features. Therefore, a brief discussion of the $Ag_{10}Te_4Br_3$ system is necessary at this point.

In $Ag_{10}Te_4Br_3$, a strand of Te_4 units, each formed by a Te_2^{2-} dumbbell and two additional Te atoms at distances much shorter than the sum of the van der Waals radii of the present atoms (see Table 7), is structurally frustrated in the

high-temperature β and α modifications. This frustration is caused by removal of silver ions that linearly coordinate the Te_4 units. This removal occurs because of increased silver mobility with temperature in their high-temperature phases. As a consequence, a superimposition of different sets of Te_4 units at different heights within the unit cell results, which cannot be resolved by the applied symmetry and translation periodicity. The situation involving the frustrated Te_4 units must be described as a Peierls-like distortion with increasing temperature. In the two high-temperature modifications (β and α) of $Ag_{10}Te_4Br_3$ in which the frustration takes place, silver is completely disordered within the cation substructure. The same situation is observed for the silver substructure over a wide temperature range in $Ag_{23}Te_{12}X$.

At this point, the somewhat unusual arrangement of the Te6a and Te6b sites must be discussed in more detail. This can easily be done by applying the same type of model that was found for $Ag_{10}Te_4Br_3$ (see Figure 3). A superimposition of two different sets of Te_4 strands is responsible for the closely neighbored, half-occupied Te positions in the struc-

(23) Bärnighausen, H.; Müller, U. *Symmetriebeziehungen zwischen den Raumgruppen als Hilfsmittel zur straffen Darstellung von Struktur-zusammenhängen in der Kristallchemie*; University of Karlsruhe and University of Kassel: Germany, 1996.

(24) Topol, L. E.; Owens, B. B. *J. Phys. Chem.* **1968**, *72*, 2106–2111.

Table 6. Site Occupancy Factors (sof), Atomic Parameters, and Isotropic Displacement Parameters (U_{iso}) for $Ag_{23}Te_{12}Br$ at 293 K

atom	Wyckoff site	sof	x	y	z	U_{iso} (Å²)
Te1a	4g	1	0.1198(2)	0.12878(18)	0	0.0433(13)
Te2a	4g	1	0.1685(2)	0.0356(2)	¹/₂	0.0489(14)
Te3a	4g	1	0.1574(3)	0.2694(3)	¹/₂	0.0663(17)
Te4a	4g	1	0.3956(2)	−0.0012(3)	¹/₂	0.0647(17)
Te5a	4g	1	0.0161(3)	0.3003(2)	0	0.0633(17)
Te1b	4g	1	−0.1272(2)	0.12083(19)	0	0.0501(14)
Te2b	4g	1	−0.0377(2)	0.1683(2)	¹/₂	0.0516(15)
Te3b	4g	1	−0.2711(3)	0.1576(2)	¹/₂	0.0730(19)
Te4b	4g	1	−0.0004(3)	0.3963(2)	¹/₂	0.0647(17)
Te5b	4g	1	−0.2986(3)	0.0138(3)	0	0.0725(19)
Te6a	8h	0.51(3)	0.3217(3)	0.1796(3)	−0.308(2)	0.069(5)
Te6b	8h	0.49(3)	−0.1821(4)	0.3206(3)	−0.3156(19)	0.063(4)
Br	4e	1	0	0	0.2448(4)	0.055(2)
Ag1	8h	0.554(17)	0.0094(7)	0.4200(4)	0.1652(13)	0.155(5)
Ag2	8h	0.435(15)	−0.4294(5)	0.0006(4)	0.101(3)	0.145(9)
Ag3	4g	0.309(18)	0.0752(7)	−0.0444(8)	¹/₂	0.067(5)
Ag4	4g	0.34(3)	0.0604(6)	0.0887(8)	¹/₂	0.25(4)
Ag5	8h	0.45(2)	0.0399(8)	0.2826(6)	−0.3437(17)	0.125(6)
Ag6	8h	0.348(19)	−0.2688(6)	0.0348(6)	−0.366(2)	0.099(5)
Ag7	8h	0.331(17)	−0.0783(6)	0.2380(7)	0.202(2)	0.100(6)
Ag8	8h	0.343(16)	−0.2816(6)	−0.0556(6)	0.3100(17)	0.095(5)
Ag9	8h	0.53(3)	−0.3812(6)	0.129(2)	−0.259(4)	0.65(4)
Ag10	8h	0.170(17)	−0.1631(14)	0.103(2)	−0.353(2)	0.161(19)
Ag11	8h	0.46(2)	0.1867(19)	0.1554(4)	−0.368(4)	0.339(18)
Ag12	8h	0.465(18)	−0.1596(5)	0.1804(10)	−0.2994(10)	0.104(5)
Ag13	8h	0.295(14)	0.0591(7)	0.2045(6)	−0.258(2)	0.109(6)
Ag14	8h	0.48(3)	−0.2427(19)	0.0668(7)	−0.2751(17)	0.35(2)
Ag15	8h	0.172(11)	0.2933(11)	0.0821(9)	−0.539(3)	0.071(10)
Ag16	8h	0.41(2)	−0.0683(9)	0.2858(6)	−0.402(4)	0.234(15)
Ag17	8h	0.36(2)	0.4313(6)	0.1162(6)	−0.332(3)	0.110(6)
Ag18	8h	0.30(2)	−0.1097(8)	0.4347(10)	−0.317(3)	0.131(9)
Ag19	8h	0.29(2)	0.0598(13)	0.1176(12)	−0.307(3)	0.195(13)
Ag20	8h	0.40(2)	−0.1331(11)	0.0849(10)	−0.369(2)	0.195(10)
Ag21	8h	0.46(2)	0.1935(6)	0.2113(10)	−0.199(2)	0.175(9)
Ag22	8h	0.493(18)	−0.2139(6)	0.2116(7)	−0.108(3)	0.278(11)
Ag23	4g	0.63(4)	0.1208(17)	0.0043(4)	0	0.27(2)
Ag24	4g	0.24(3)	0.0017(11)	0.1059(8)	0	0.234(13)
Ag25	8h	0.317(16)	0.2234(7)	0.0723(7)	−0.8110(14)	0.092(6)
Ag26	8h	0.14(3)	−0.0542(16)	0.2132(10)	−0.835(3)	0.42(2)
Ag27	8h	0.44(2)	0.1585(17)	−0.0029(17)	−0.180(3)	0.40(2)
Ag28	8h	0.396(18)	−0.0045(5)	0.1405(12)	−0.1456(18)	0.190(11)
Ag29	4g	0.40(4)	0.4016(10)	0.155(4)	¹/₂	0.44(5)
Ag30	4g	0.31(3)	−0.1348(9)	0.3986(12)	¹/₂	0.120(11)
Ag31	4g	0.42(4)	0.245(3)	0.2038(13)	0	0.47(4)
Ag32	4f	0.279(12)	0	¹/₂	0.254(3)	0.149(11)
Ag33	8h	0.354(17)	0.2386(11)	0.3651(5)	−0.383(2)	0.121(6)
Ag34	8h	0.33(2)	−0.3786(14)	0.2448(12)	−0.327(2)	0.192(14)
Ag35	4g	0.6(2)	0.1366(8)	0.3877(6)	¹/₂	0.32(2)

ture model for $Ag_{23}Te_{12}X$. This section of the structure model, which is characterized by predominantly covalently bonded tellurium, therefore represents only an average structure. For $Ag_{23}Te_{12}X$, a disordered silver substructure was found over the whole temperature range from 293 to 140 K, and there is no way to prove the postulated model by a phase transition with tellurium and silver ordering as in $Ag_{10}Te_4Br_3$. An overview of the interatomic Te−Te distances in the Te_4 units in $Ag_{10}Te_4Br_3$ and $Ag_{23}Te_{12}X$ is given in Table 7. It is remarkable that $Ag_{23}Te_{12}Br$ features two structurally different types of Te_4 units. In one set of dumbbells, the Te−Te distance is 2.8 Å, whereas in the other one, this distance is clearly elongated, with a bond length close to 3 Å. Upon elongation of the Te−Te dumbbell, the additional contact to the neighboring Te position becomes shorter (Table 7). This finding points toward the formation of an equidistant arrangement of tellurium within the Te_4 strand, which was also identified as an intermediate step in the phase transitions to the high-temperature phases of $Ag_{10}Te_4Br_3$. The coexist-

ence of shorter and longer dumbbells is comparable to the situation in β-$Ag_{10}Te_4Br_3$ yet even more pronounced. Both aspects, the large amount of disorder in the silver substructure and the averaged polyanion substructure, also lead to short Ag−Te distances (less than 2.5 Å), which are caused by the aforementioned effects.

The diversification of Te−Te distances, which is in accordance with more realistic bond distances of 2.8 Å (compared with 2.91 Å for the $P4/mnc$ model), substantiates the choice of the lower-symmetry orthorhombic space group $Pnnm$ instead of the supergroup $P4/mnc$. The present case is a nice example of an averaged polyanion substructure determined by X-ray diffraction experiments that has nothing to do with the real structure. Analysis of the real structure requires the use of high-resolution transmission electron microscopy (HRTEM) experiments. Unfortunately, the silver(I) (poly)chalcogenide halides are not stable in the presence of the electron beam under HRTEM conditions, making such experiments impossible.
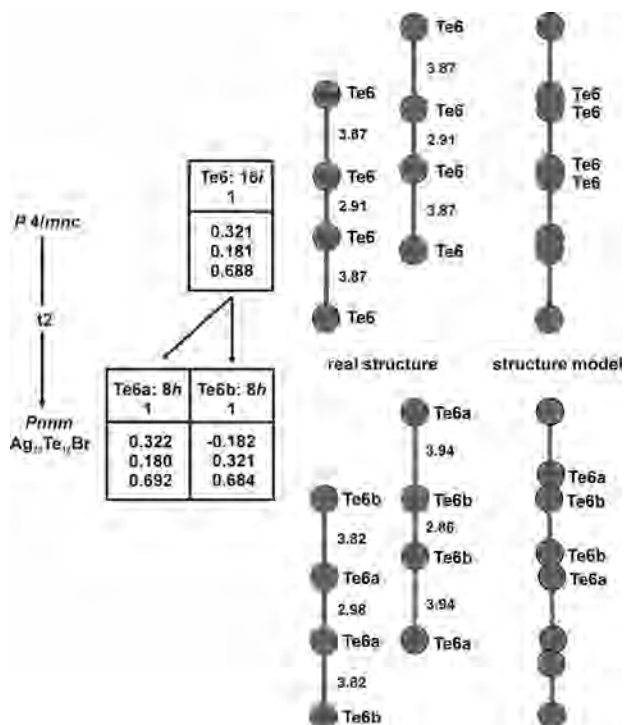
Figure 3. Section of the group−subgroup scheme according the Bärnighausen formalism[22,23] for $Ag_{23}Te_{12}Br$. The 16i site of $P4/mnc$ splits into two 8h sites in $Pnnm$. On the right-hand side, a model of two Te_4 units at different heights within the unit cell is given for each space group. A superimposition of these units creates the half-occupied Te positions in the respective structure models.

The halide substructure consists of strands which run parallel to the c axis. The silver atoms are distributed over

a large number of partially occupied sites. In the vicinity of the halide ions, a smaller density of silver positions can be observed (see the bottom-left panel of Figure 4). This circumstance is comparable to the situation found in other silver chalcogenide halides and (poly)chalcogenide halides that we have investigated previously.[4,5]

Electrical Properties. The pronounced disorder in the silver substructure over a broad temperature range encouraged us to investigate the electrical properties of $Ag_{23}Te_{12}Br$. An Arrhenius-type plot of the specific ion conductivity as a function of reciprocal temperature is given in Figure 5. A discontinuity of the slope was observed at 340 K. Thermal analyses did not show any hints of a possible phase transition in the temperature range under discussion. Further electrochemical measurements are planned in order to obtain deeper insight into the electrical properties and the origin of the discontinuity. The measurement proves that silver is mobile in $Ag_{23}Te_{12}Br$, but the observed values were 1.5 orders of magnitude smaller than those for $Ag_{10}Te_4Br_3$. Activation barriers were determined from the slope of the curve after linear regression, and the calculated values fell between 0.54 and 0.98 eV. The complete data set is summarized in Table 8.

Comparison of the ion conductivity of $Ag_{23}Te_{12}Br$ near room temperature ($\sigma = 1 \times 10^{-5}$ Ω^{-1} cm^{-1}; see Table 8) with that of AgBr ($\sigma = 1 \times 10^{-6}$ Ω^{-1} cm^{-1})[18] reveals an increase of 1 order of magnitude. A small admixture of halide to binary silver telluride not only led to a completely new structure type but also significantly decreased the resulting ion conductivity of the new compound. In relation to other highly ion conducting materials such as β-Ag_3SBr (~5 ×
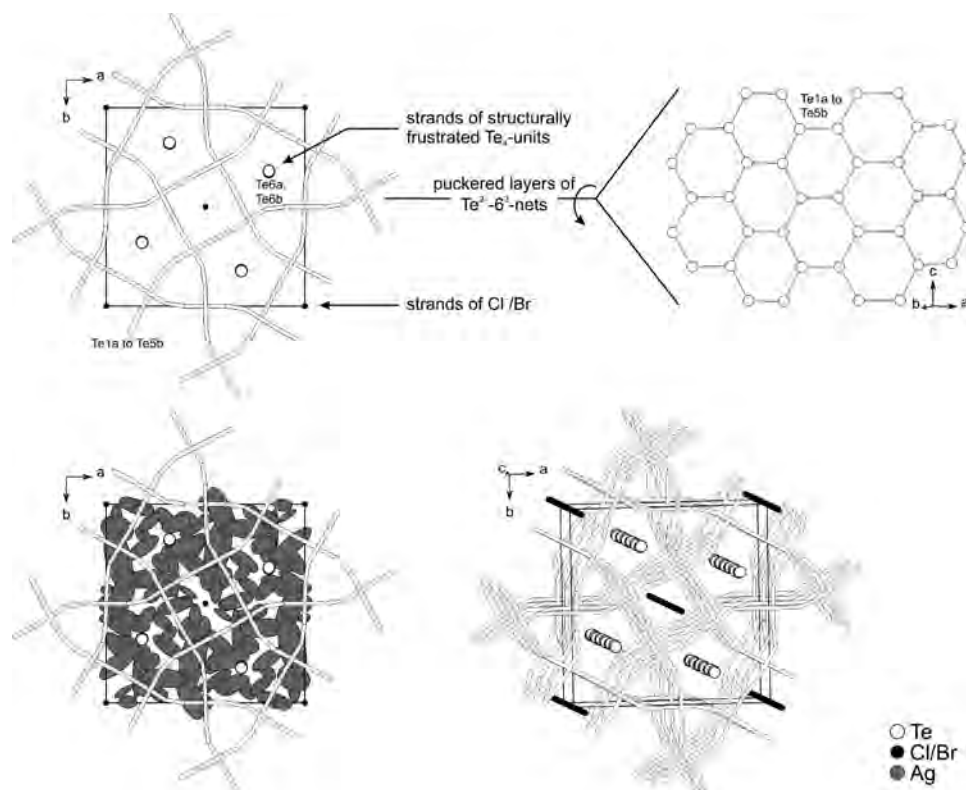
Figure 4. Crystal structure of $Ag_{23}Te_{12}X$ (X = Cl, Br). Tellurium forms puckered 6^3-nets which interpenetrate each other. Strands of structurally frustrated Te_4 units and halide ions run parallel to the c axis. The silver atoms are distributed over a large number of partially occupied sites.

Table 7. Interatomic Te−Te Distances in the Te−(Te₂²⁻)−Te Units of Various Silver (poly)Chalcogenide Halides

compound	T (K)	d_{Te-Te} (Å)[a]		type	reference
		(Te₂²⁻)	(Te₂²⁻)−Te		
α-Ag₁₀Te₄Br₃	410	2.898(8)	3.809(6)	frustrated	6
β-Ag₁₀Te₄Br₃	340	2.877(9)	3.835(8)	frustrated	6
		2.793(3)	3.653(3)	ordered	6
γ-Ag₁₀Te₄Br₃	293	2.793(2)	3.604(2)	ordered	6
δ-Ag₁₀Te₄Br₃	223	2.805(1)	3.586(1)	ordered	6
Ag₂₃Te₁₂Cl	293	2.81(1)	3.89(1)	frustrated	this work
		2.89(1)	3.81(1)	frustrated	
Ag₂₃Te₁₂Br	293	2.86(2)	3.94(2)	frustrated	this work
		2.98(2)	3.82(2)	frustrated	
Ag₂₃Te₁₂Br	150	2.80(2)	3.97(1)	frustrated	this work
		3.01(1)	3.76(1)	frustrated	
Ag₂₃Te₁₂Br	100	2.80(1)	3.97(2)	frustrated	this work
		3.02(2)	3.81(1)	frustrated	

[a] Standard deviations are given in parentheses.
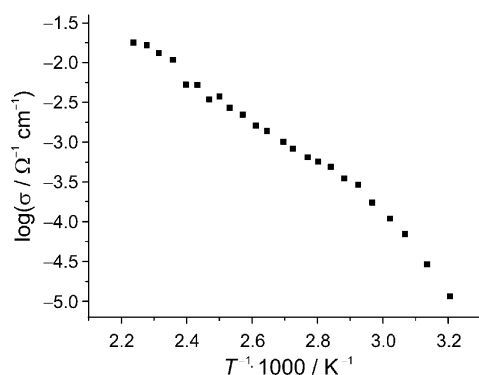
Figure 5. Arrhenius-type plot of the specific ion conductivity of Ag₂₃Te₁₂-Br.

10^{-3} Ω^{-1} cm^{-1}),[19] β-Ag₃SI (1 × 10^{-2} Ω^{-1} cm^{-1}),[20] γ-Ag₁₀Te₄Br₃ (7.5 × 10^{-4} Ω^{-1} cm^{-1} at 301 K),[6] Ag₇I₄PO₄ (1.9 × 10^{-2} Ω^{-1} cm^{-1}),[21] and RbAg₄I₅ (2.1 × 10^{-1} Ω^{-1} cm^{-1}),[1] the observed room-temperature conductivity is 2−5 orders of magnitude smaller. On one hand, this finding clearly substantiates the potential of the new class of silver (poly)-chalcogenide halides, but on the other hand, it also shows that not every (poly)chalcogenide halide can compete with the best-known ion conductors. Nevertheless, the existence of Ag₂₃Te₁₂X encourages us to improve our research activities within the ternary coinage-metal−chalcogen−halogen systems in order to find new compounds with the goal of optimizing the electrical properties. In contrast to the thermodynamically instable compounds MAg₄I₅ (M = Rb, K, NH₄)[1,23] at room temperature, the title compounds showed no decomposition in air or moisture over a period of 1 month, and the silver dynamics over a broad range of temperatures make them potential candidates for room- or low-temperature applications.

Conclusion

Ag₂₃Te₁₂Cl and Ag₂₃Te₁₂Br feature both covalent and ionic motifs in their anionic substructures and thus

Table 8. Specific Ion Conductivities Derived from Electrochemical Measurements on Ag₂₃Te₁₂Br

T (K)	σ_{ion} (Ω^{-1} cm^{-1})	T (K)	σ_{ion} (Ω^{-1} cm^{-1})
312	1.2 × 10^{-5}	378	1.4 × 10^{-3}
319	2.9 × 10^{-5}	383	1.6 × 10^{-3}
326	7.0 × 10^{-5}	389	2.2 × 10^{-3}
331	1.1 × 10^{-4}	395	2.7 × 10^{-3}
337	1.7 × 10^{-4}	400	3.8 × 10^{-3}
342	2.9 × 10^{-4}	405	3.4 × 10^{-3}
347	3.5 × 10^{-4}	411	5.3 × 10^{-3}
352	4.9 × 10^{-4}	417	5.3 × 10^{-3}
357	5.7 × 10^{-4}	424	1.1 × 10^{-2}
361	6.4 × 10^{-4}	432	1.3 × 10^{-2}
365	8.3 × 10^{-4}	439	1.7 × 10^{-2}
369	1.0 × 10^{-3}	447	1.8 × 10^{-2}

represent two new members of the silver (poly)chalcogenide halide structure family. Both compounds crystallize isostructurally in space group *Pnnm*. Systematic twinning was observed along with complex disorder phenomena within the (poly)telluride substructure that resemble the situation previously found[6] in the high-temperature polymorphs of the related compound Ag₁₀Te₄Br₃. Thermal analyses and crystal structure determinations at various temperatures gave no evidence for the existence of further polymorphs of either the chloride or the bromide compound. Nearly equal composition and crystallographic parameters as well as a comparison of the structure models suggest a high probability that "Ag₂₁Te₁₀Br" reported by Schnieders[9] and Ag₂₃Te₁₂Br described in this work are the same compound. Electrochemical measurements showed that silver is mobile in Ag₂₃Te₁₂Br; the ionic conductivity was 1.5 orders of magnitude smaller than that of Ag₁₀Te₄Br₃.

The Ag₂₃Te₁₂X series is the second set of representatives within the phase field AgX−Ag₂Q−Q (X = halide; Q = chalcogenide), following the previously reported Ag₁₀Q₄X₃ family. Both members of this phase field are characterized by comparable polytelluride substructures featuring a Peierls-distorted chain of predominantly covalently bonded tellurium.

Supporting Information Available: Crystallographic information files for Ag₂₃Te₁₂Cl at 298 K and Ag₂₃Te₁₂Br at 100, 150, and 293 K and tables of anisotropic displacement parameters, selected interatomic distances, and additional crystallographic data. This material is available free of charge via the Internet at http://pubs.acs.org.

IC701988U